JOURNAL OF MATERIALS SCIENCE **36** (2001) 4779–4795

Thermal analysis of slow cooled copper-tin alloys

N. N. ACHARYA
Department of Metallurgical & Materials Engineering, Indian Institute of Technology, Kharagpur 721302, India
E-mail: nnacharya@metal.iitkgp.ernet.in

When elemental copper and tin powders alloy to form bronze, in the molten state or by diffusion in the solid, they go through several reactions and transformations, as given in the Cu-Sn Phase Diagram. It is of interest, especially for powder metallurgical applications, to know their dilation effects on the compacts as they are heated during sintering. Attempts in this article have been made to fingerprint these reactional and transformational related dilations, using Thermo-mechanical analysis (TMA) on slow-cooled synthesized alloys of various compositions. Differential thermal analysis (DTA) and metallography back up the results. It is seen that except for the eutectoid formation of β from α and γ (during heating), all transformations have a dilation effect.

1. Introduction

The production of self-lubricated bearings has been underway since the 1920's when they were first developed in processes patented by Loewendahl [1] and Gilson [2, 3]. Others later improved their process, mainly by the utilization of homogeneous blends of elemental copper and tin powders, often with additions of graphite and ad-mixed lubricants like zinc stearate. The use of pre-alloyed atomized powders in premix formulations has also been attempted much later. However, considering the economics, it became a more common practice to use elemental powder mixes for production of these bearings.

One of the important requirements in bearing production is the accuracy of the final dimensions, and their reproducibility from batch to batch. This is not always achieved, as there usually is a slight distortion after sintering. To overcome these deviations from the specified final dimensions, the sintered bearings are invariably sized or re-pressed through the sizing die. Apart from incurring extra expenses thereby, re-pressing also affects the various bearing properties, particularly its surface pore structure, which is of great importance. Re-pressing is therefore best avoided if possible, or its effects minimized as much as possible.

It is quite expected that the distortions and dimensional changes that occur in the copper-tin system be influenced by the structure formation behaviour during sintering. An in-depth understanding of it is therefore required. When elemental powders are used, the copper-tin system (Fig. 1) [4] has to be studied over the entire range, i.e., from 0 wt%Sn to 100 wt%Sn. This is because, in the green state, pure copper surrounds pure tin particles. These two elements go through several stages of alloying to give the final structure, which is usually a near homogeneous α - bronze. It should also be remembered that the phase diagram is just a guide to understand the alloying behaviour, as the kinetics of sintering is not at all slow, and therefore corresponds to a non-equilibrium situation. Besides this, all reactions and transformations during sintering are studied while heating the powder specimens, and not during their cooling.

Berry [5] published the effects of various materials and process parameters affecting the growth of bronze bearings prepared from water atomized copper powders. He also studied the role of prealloyed powders in various mixes along with other factors influencing the dimensional changes. According to him, the development of growth, (i.e. expansion of the samples), during sintering can be divided into four stages. First, there is growth upto 750°C, which is followed by constant dimensions between 750 and 800°C. There is again a rapid growth between 800 and 810°C; afterwhich there is a growth-reduction (decrease in the rate of growth) above 810°C. Further, according to him, the rise in growth between 400 and 750°C is a function of tin-diffusion. Its magnitude of growth is increased by three factors: viz., the oxide content of copper, an addition of graphite (particularly synthetic graphite), and a decrease in the reducing potential of the sintering atmosphere. In this region, the growth effect of tin-diffusion overrides the shrinkage factor due to the sintering mechanism. Between 750 and 798°C, the growth tends to be stable, or sometimes, a slight reduction occurs. This, he explains, is because diffusion of tin is still in progress, tending to create a growth effect, but the shrinkage effect of the sintering mechanism is more pronounced because of the higher temperature. Thus, there exists a neutralizing effect of the two forces. At the peritectic temperature of 798°C a liquid phase is produced, the quantity of which depends on the degree of various diffusions before this temperature is reached. He stipulates that the rise in growth at this temperature is due to the rapid diffusion of tin. His results also show that the growth-rise is enhanced only when the specific

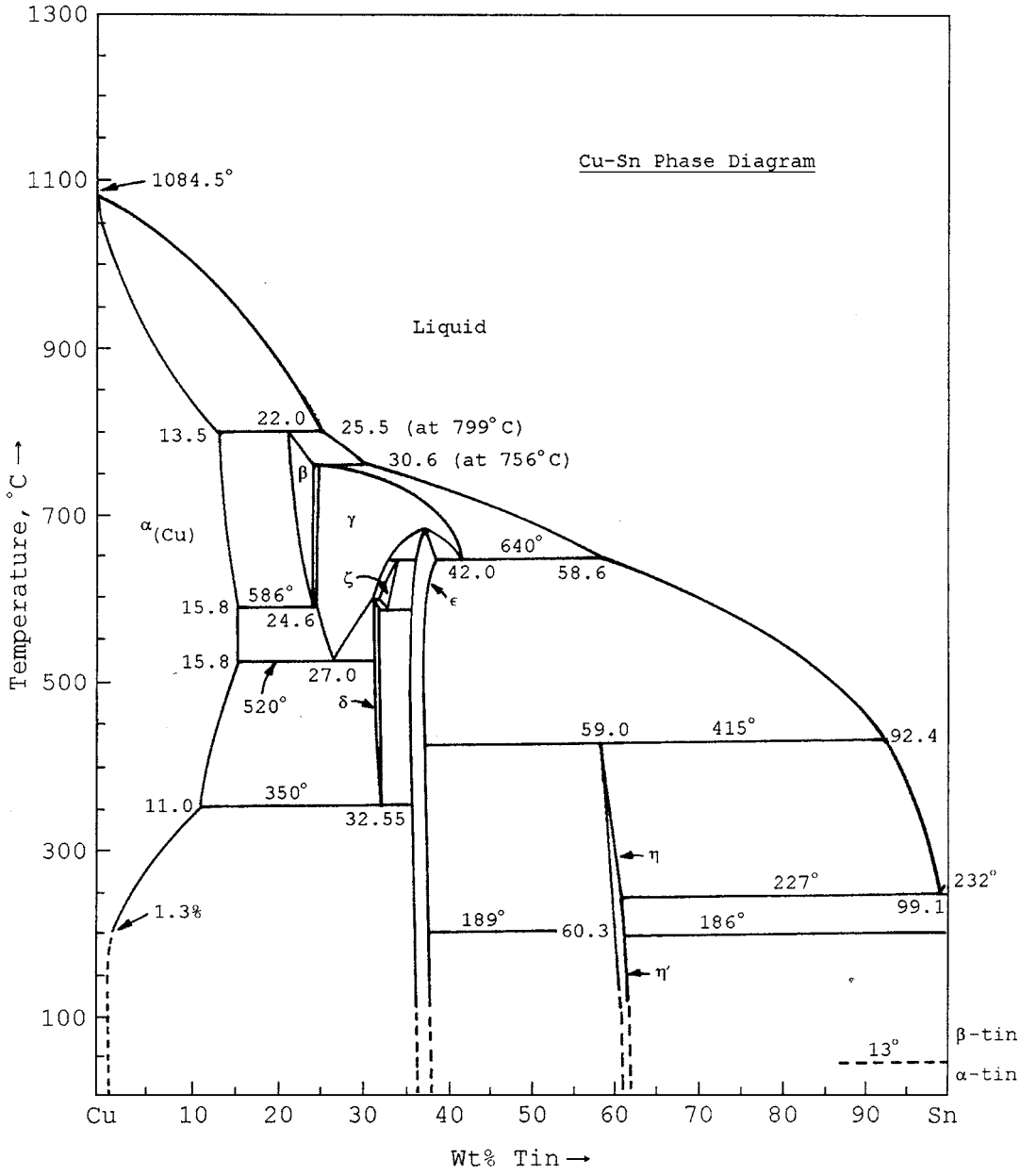

Figure 1 Equilibrium phase diagram of copper-tin system.

surface area of the tin powder is decreased. He finds a decrease in growth beyond 810°C, at which point a homogeneous alloy has been achieved. The growth is retarded by the presence of graphite, as well as when the sintering atmosphere is lean, (or less reducing). According to him, since at this stage, it is a situation of solid-state sintering, the presence of graphite or other surface impurities decrease the effective surface area.

Mitani [6] analyzed the phenomenon of abnormal growth at 798°C. According to him the peritectic reaction at this temperature, coupled with a release of gases, is the cause for such an expansion. Peissker [7], worked on various combinations of prealloyed bronze and/or elemental tin and reduced as well as unreduced copper powders. He analyzed the role of surface area of copper powder, the lubricant, and the effect of sintering above and below the highest peritectic temperature on growth characteristics through dilatometric plots. According to him, premixes containing only prealloyed particles do not exhibit any expansion at the peritectic temperature.

Regarding the characteristics of growth, Koehring [8] reported that an addition of 1.5 wt% of graphite to the copper-tin mix could bring about a near-net shape in the sintered compact with zero dimensional change. He found that an addition of less than 1.5 wt% graphite would cause shrinkage, whereas with more than 1.5 wt% graphite, a net growth could be seen in the sintered compacts. Thus, apart from adding graphite to the copper-tin mix for reducing static friction at the bearing surface, it was thought that it could also be used as a controlling factor for dimensional stability during sintering.

Bose *et al.* [9–14] showed that the powder characteristics, as well as the process variables have a remarkable influence on the sintering behaviour and the subsequent properties of the sintered compact. Therefore, the question arises whether addition of this 'optimum' amount of 1.5 wt% of graphite for dimensional stability holds good under all the varying conditions of powder characteristics and process variables. Considering their work,

it is quite expected that the dimensional stability, or instability, would depend on a number of parameters, such as the material and processing conditions.

To study dynamic changes in the dimensions of a specimen with temperature a dilatometer may be used. However, in the case of powder metallurgical copper-tin samples, the compacts are not only porous, but also soft, with additional complications due to the formation of transient liquids at various stages. The dilatometric analysis therefore could depend largely on the equipment itself. The ideal equipment for studies on this system would be a dilatometer where the probe applies no pressure on the specimen. Thus, an earlier work with a fabricated capacitance-bridge dilatometer [15–17] showed that except for a short span short span between 635°C and 645°C, when ζ dissociates into $\gamma + \varepsilon$, almost every reactions in the Cu-Sn system has some influence on the ΔL of the compacted powder specimen. It was also observed that due to the presence of pores, these influences, especially those related to the reactions involving transient liquid, were often detected after a delay. This again depended on the powder characteristics and the process variables.

While this work with a capacitive-bridge dilatometer noticed a number of dilation peaks, both expansion as well as shrinkage, the dilation plots obtained by Patel [18, 19], Kohno [20], and Savitiskii [21] showed continuous expansion with temperature until 650°C, followed by shrinkage beyond it. No significant changes were seen at other temperatures.

Although treating the earlier work by the author of this article as an approximate picture of the dilation characteristics vis-a-vis the intrinsic changes that occur during sintering, the analysis of data obtained from the fabricated capacitive-bridge dilatometer was quite cumbersome. Thus, such equipment does not have much of practical use in industry where time is valuable and speed is of the essence. It is therefore worthwhile to compare this earlier data with those obtained from conventional commercially available dilatometric equipment.

The elemental powders used in a Cu + 10 wt%Sn compact are of various sizes, as can be seen in a p/m green compact, (Fig. 2). Every tin particle acts as a reaction site until they begin to "join hands". Therefore, however homogeneous the mixture is, the inevitable size variation of tin particles renders that the reactions at each of the sites are at different stages of completion. Thus, looking at the situation "globally", several reactions would thus occur simultaneously, [11–13], each reaction having its own characteristic thermal effect. Like all thermal analysis plots, TMA plots too would give the algebraic sum of the dilations of all the individual reactions. Unless the exact microstructural scenario in the compact at a particular time and temperature is known, it is not easy to ascribe a particular peak or hump in the TMA plot to a particular reaction in the equilibrium phase diagram. The microstructure of powder compacts can be frozen at various stages of sintering, but to establish the dilation behaviour with respect to each of the reactions or transformations that could occurs in a copper-tin system it becomes necessary to fingerprint them.

This fingerprinting work is best carried out on synthesized alloys, and not on sintered compacts. The advantage of using solid alloys is that it makes the interpretation of TMA plots much easier. Here, one would be dealing with an alloy of a specific composition going through a single reaction at a time, unlike in the case of sintered compacts.

Since the changes of slopes due to these transformations are often gradual or minute, it is easier to interpret the plot of its derivative with respect to time, [22]. Apart from this, it is also useful to take the help of Differential Thermal Analysis, DTA, along with metallography to understand the dilation changes with respect to any

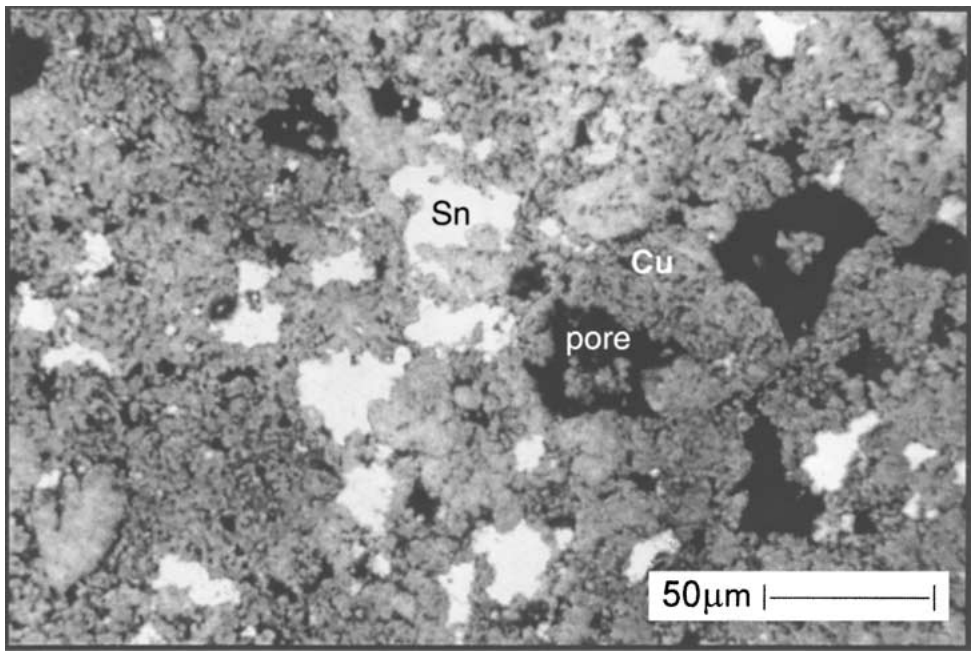

Figure 2 Microstructure of Cu + 10 wt%Sn green compact.

particular intrinsic change. The peaks in the DTA plot could confirm the results obtained from TMA, whereas metallography would give a better understanding of the actual phases present at a particular temperature.

The main objective of this work, therefore, is to establish the effect of each of the reactions in the Cu-Sn system on dilation, (dilation-fingerprinting). DTA and metallography of the pre-analysis samples have supported the results.

2. Experimental details

As this work is carried out to assist an in-depth study of dilation during sintering powder metallurgical Cu-Sn bush bearing, it would have been ideal if the geometry of the actual bush bearings were used for this fingerprinting work. The dimensional changes in both axial and radial directions would then have been determined. However, there is no dilatometer available commercially that accepts such specimen geometry.

Therefore, cylindrical specimens were used, and the results obtained from them were extrapolated to actual changes that take place in P/M bush bearings during sintering.

2.1. The equipment and alloy preparation

Before proceeding with the dilation characteristics of alloys in Cu-Sn system (and subsequently Cu + Sn and Cu + Sn + C powder systems that will be dealt with in sequels to this article), the viability of TMA (carried out on Shimadzu DT-30 in this work) as a tool needed to be first established. In this TMA unit, a thin long cylindrical probe (quartz rod with a diameter of 3 mm) is placed lightly on top of the specimen, (Fig. 3). The change in length of the specimen as it is heated causes the probe to move up or down vertically. This movement is converted into electrical pulses by a Linear Voltage Differential Transformer (LVDT) and subsequently amplified and recorded on a chart. In order to achieve some stability a small load is placed on a pan at the top end of the probe. This load is, however, effective as far as P/M bronzes are considered. Bronze is quite soft, and particularly at high temperatures, such as above 600°C, there is a likelihood of their compacts being deformed under pressure.

The accuracy and the sensitivity of this unit was checked by heating a copper specimen, and a Cu-28-wt%Sn bronze specimen upto 850°C respectively. This work has been elaborated in [22, 23]. It has been seen that the thermal expansion of copper is measured accurately, and the eutectoid transformation, $(\alpha + \delta) \rightarrow \gamma$ at 520°C, during heating, is clearly detected. Its derivative, i.e., the rate at which the dilation changes with temperature, $(\mathrm{d}\Delta L/\mathrm{d}t)$, shows the eutectoid transformation more clearly with a couplet of a minima and a maxima. The starting point of the minima is the onset temperature of the eutectoid transformation (or any such prominent reaction.)

Thermal Analysis was carried out during heating of the specimens, and not during cooling. However, the microstructural studies were carried out on cooled alloys as they gave the scenario of the system before TMA

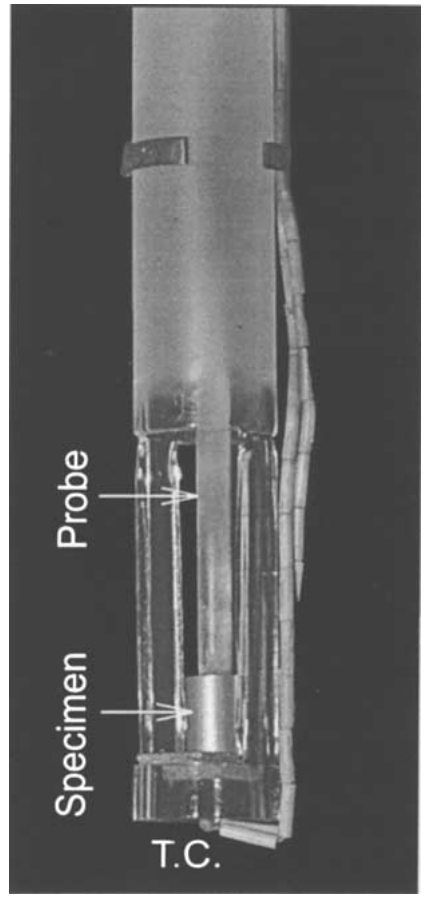

Figure 3 TMA unit showing the sample, the probe, and the thermocouple.

and DTA were carried out. Thus, all the specimens—for microstructural studies, TMA and the DTA were subjected to the same heat treatment. They were melted, and then cooled in the furnace, taking about 10 hours from 1200°C to 60°C. By this time, all the reactions in the Cu-Sn system would have undergone completion, (that is kinetically speaking, for the α phase and the δ phases are stable at room temperature). The effect of rapid cooling on TMA, DTA and microstructure is not included in this article. A separate article would be submitted on this.

For carrying out this thermal analysis work, sixteen different compositions were chosen (A0–A15). While A0 was electric grade copper and A15 was commercially pure tin with trace impurity lead, A1 through A14 were so chosen as to coincide with significant compositions in the Cu-Sn system.

First, requisite amounts of copper and tin were melted together at 1200°C in an induction furnace to achieve good homogenization. Alloys with tin more than 30% by weight could be easily pulverized, and several small bits of each were taken for chemical analysis. Alloys with less than 30-wt%Sn were drilled at several places, and these drillings were used to find its composition. This random sampling from the entire bulk of the material enabled to check for any inhomogeneity or stratification along the sample depth.

After chemical analysis of the master alloys, they were pulverized, and their compositions were fine-tuned by adding the deficit element. This process of

melting and chemical analysis was repeated until the desired compositions were obtained. Chemical analysis showed that the actual compositions finally achieved were:

A0 100Cu (electric grade Cu),
A1 89Cu-11Sn,
A2 83Cu-17Sn,
A3 74.5Cu-25.5Sn,
A4 72Cu-28Sn,
A5 67.5Cu-32.5Sn,
A6 66Cu-34Sn,
A7 62Cu-38Sn,
A8 57Cu-43Sn,
A9 50Cu-50Sn,
A10 40Cu-60Sn,
A11 29Cu-71Sn,
A12 21Cu-79Sn,
A13 10Cu-90Sn,
A14 5Cu-95Sn, and
A15 100Sn (commercial grade, with trace lead).

From the above samples, A3 (74.5Cu25.5Sn) was also given a special heat treatment. It was homogenized, first at 600°C and then at 580°C for 8 hours and 12 hours respectively, followed by rapid cooling. This was done to get the $(\alpha + (\alpha + \delta))$ eutectoid of equilibrium composition that should give β while heating.

Similarly, A10 (40Cu60Sn) was homogenized at 390°C for 24 hours and cooled rapidly. This was done to get a substantial amount of η phase in the structure. During earlier work [25], it has been found that η is a difficult phase to be obtained by casting, as it is product of a peritectic reaction during cooling a melt. Rapid solidification of a melt with a composition of Cu+60wt%Sn would only produce more of ε and Sn, rather than the η phase.

2.2. Specimens for thermomechanical analysis of Cu-Sn alloys

For making TMA specimens a graphite block with several holes of 4 mm diameter drilled into it was used. Crushed bits of these alloys were packed into these holes. The block with the alloys was heated in hydrogen to 1200°C, and was then allowed to cool in the furnace. The specimens obtained were cylindrical. Their top and the bottom surfaces were filed to make them flat.

Considering that all compositions of Cu-Sn bronze soften remarkably as the temperature reaches the liquidus or 600°C, whichever is earlier, slight eccentric placement of the quartz probe could lead to buckling. In order to avoid this, the specimen-length for this work was kept between 9 and 11 mm. Again, in order to avoid any pronounced temperature distribution in the specimen, (in spite of it being small and highly thermally conductive or thermally thin), the diameter was kept at 4 mm. This small diameter also assisted in placing the probe as close to the central axis as possible. Once more, as the length of these specimens varied between 9 mm and 11 mm, they were short enough to receive homogeneous heating. In fact, since bronze is a good conductor, the specimen-size chosen for the work ensured no heat-transfer problems. The TMA runs were carried out in commercial purity argon at the rate of 10°C/minute. A load of 2g was used for all runs [22]. The derivative was measured at 4 mV/minute. (Shimadzu DT30 recommends specimen to have a diameter upto 8 mm, and a length between 5 mm and 20 mm, with a load of 2g on the specimen. For a probe with a diameter of 3 mm, this load applies a pressure of 28 cN/cm^2.)

2.3. Specimens for differential thermal analysis of Cu-Sn alloys

The specimens for DTA work were made in a similar way as the TMA samples. A small quantity of each of the alloys was taken in the holes in the graphite block, and heated to 1200°C in hydrogen. The specimens were furnace-cooled to room temperature just as in the case of TMA specimens.

Differential Thermal Analysis was done on the Shimadzu unit in Argon, also at 10°C/minute. Pure alumina powder was used as the reference, and the small specimens were filed as flat as possible to achieve a better thermal contact compared to just a few point contacts, (Fig. 4). The specimen weights were kept between 30 mg and 120 mg. More material would have given a larger $\pm\Delta H$. However, at the same time, due to the slight temperature difference between the surfaces to the core, sharp peaks due to the intrinsic changes would have flattened to a small extent.

Figure 4 DTA unit, showing the reference and the specimen under study.

2.4. Specimens for metallography of Cu-Sn alloys

Alloys for metallography were made in a similar manner, likewise to the DTA and TMA specimens—in a graphite block at 1200°C. The entire set of alloys was mounted in cold setting resin. After preparing the metallographic surface by paper grinding and diamond polishing, they were etched in acidified potassium dichromate solution, [25]. The formula is given below:

Potassium dichromate, $K_2Cr_2O_7$	2 g
Sulphuric acid conc., H_2SO_4	8 cc
Water, H_2O	100 ml

25 ml of the above with 1 ml of Hydrochloric acid (conc.), HCl, was used for etching.

To improve the contrast between the various phases, the etched specimen were colour tinted using complex thiosulphate reagent [26]. The formula is:

Sodium Thiosulphate [$Na_2S_2O_3$]	240 g
Lead Acetate [$Pb(CH_3COO)_2 \cdot 3H_2O$	24 g
Citric Acid [$C_6H_8O_7 \cdot H_2O$]	30 g
Distilled water [H_2O]	1000 ml

The chemicals are to be mixed in the given order. The reagent has an incubation period of about 24 hours, and the black & white precipitate that forms should be filtered off.

3. Results

There are several reactions over the entire range of tin, viz., peritectic reactions, peritectoid reactions, eutectic, eutectoid, a metatectic reaction and a congruent transformation. The thermal analysis of these reactions for powder metallurgical purpose have to be studied during heating, rather than cooling, when sintering takes place as the temperature of the green compact is raised. The dilation characteristics determined by TMA is the external manifestation of the various intrinsic changes that take place. The latter is best recorded by DTA. Thus, it is felt that the TMA plots are better understood in the light of the corresponding DTA. Again, as DTA and TMA are influenced by the phases participating in a reaction, the study is complete only when the micro-structural scenario in each case is found from the synthesized alloys that have been cooled.

The DTA plots are given in Fig. 5. Thermo-mechanical analysis plots of alloys of varying compositions are shown in Fig. 6. The derivative plots of TMA ($d\Delta L/dt$ at 4 mV/minute) are shown in Fig. 7. As the variations of the slopes are very subtle and gentle in the TMA plots, most of the temperatures are marked on the derivative plots.

3.1. A0

The DTA plot for A0 (pure copper) done in argon does not show anything remarkable, except for a slight drift in the background, attributed to the inevitable minute thermal imbalance in the tuning of the equipment. The absence of peaks indicates the obvious that copper does not undergo any transformation in the inert atmosphere, when heated to a temperature within the range under consideration. Indeed, the microstructure for A0, (Fig. 8), shows a single-phase structure with some annealing twins.

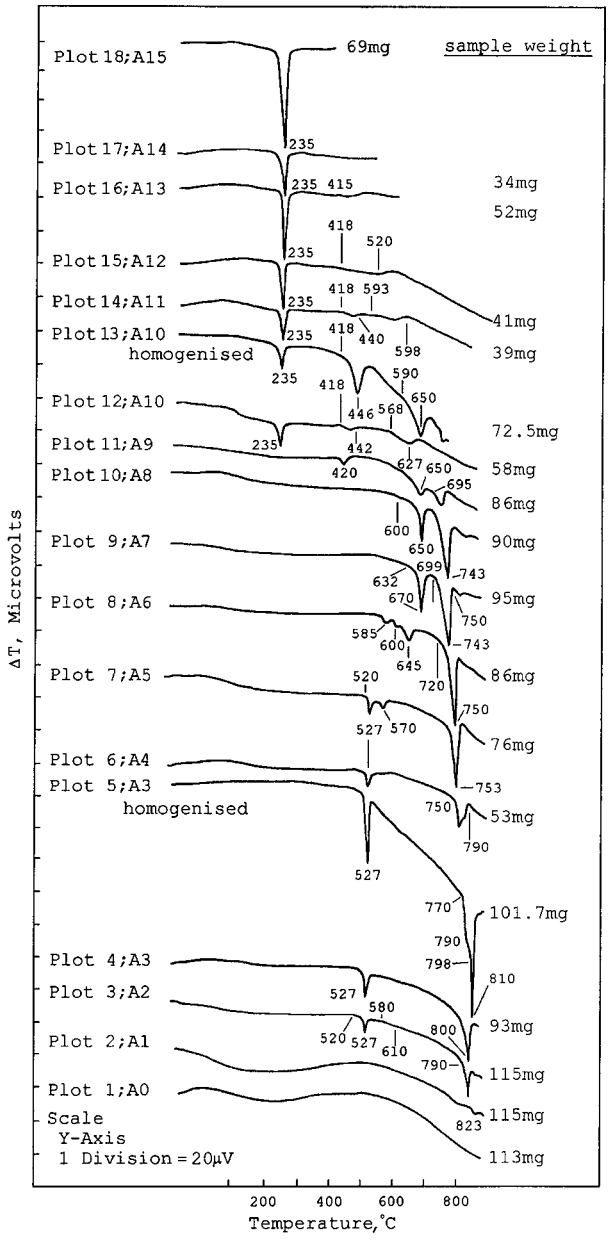

Figure 5 DTA plots of the synthesized copper-tin alloys.

The TMA plot of sample A0 shows an expansion that is almost linear with rise in temperature. For a specimen that has a length of 11.08 mm at 30°C, it shows an overall expansion of 154 μ until 850°C. This gives an average coefficient of thermal expansion of $0.0000172°C^{-1}$, which is quite close to the reported value of $0.0000167°C^{-1}$, [23].

3.2. A1

The microstructure of this alloy, (11%Sn), (Fig. 9), shows α- phase, and spherodised pores that were originally inter-dendritic. Micro-twins are seen near the pores. The DTA plot for A1 also shows no transformation. This indicates that alloy is solid α- phase before its liquefaction begins at about 823°C. In concurrence with the DTA, the TMA also shows no change in the rate of dilation until the alloy cuts the solidus at about

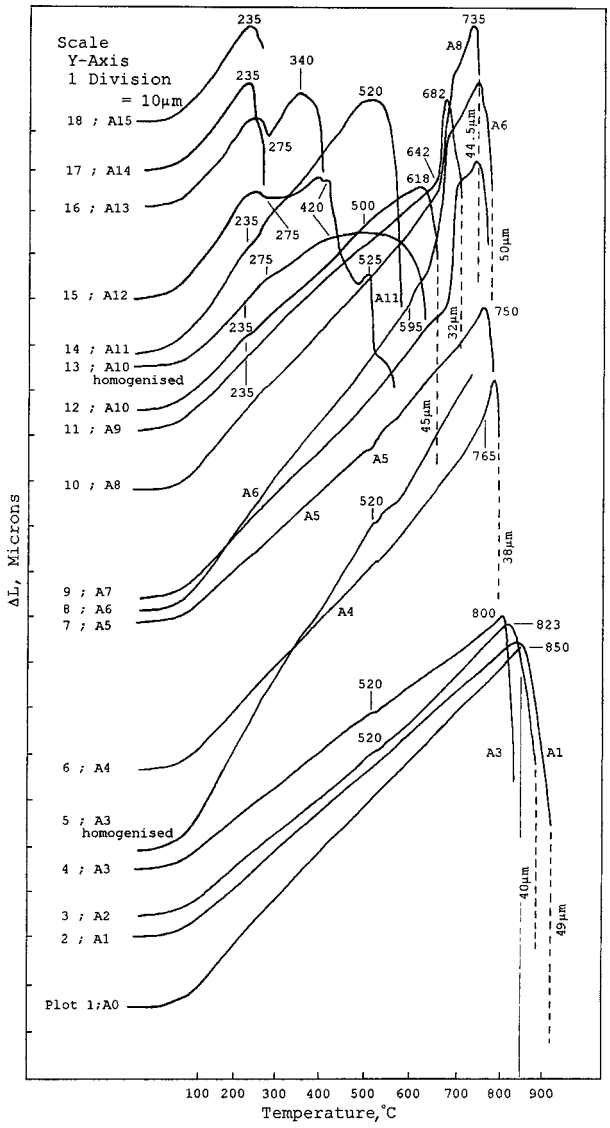

Figure 6 TMA plots of the synthesized copper-tin alloys.

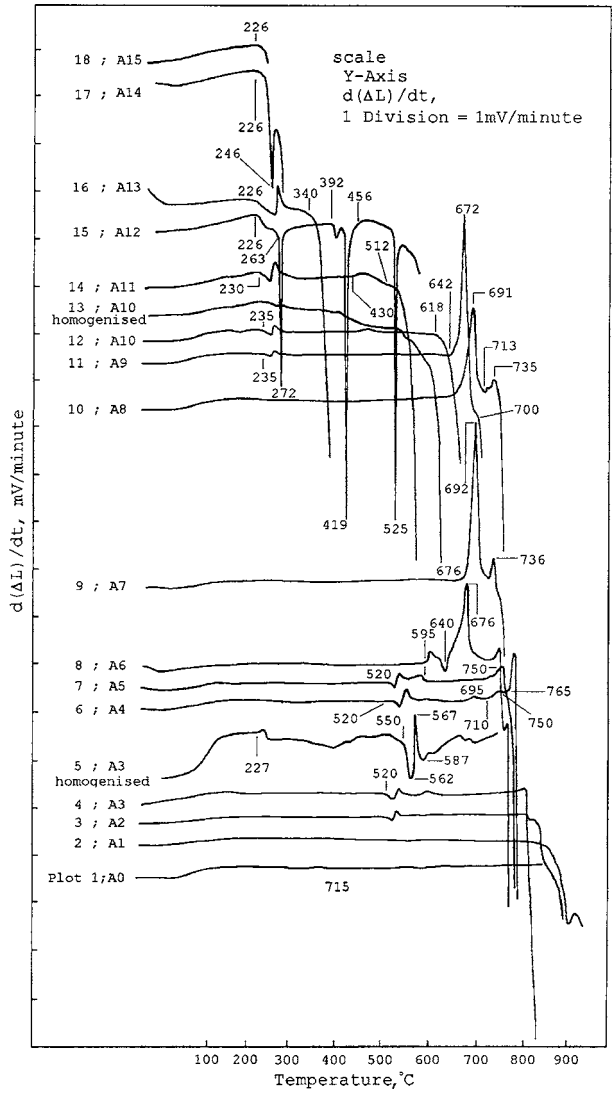

Figure 7 TMA derivative plots of synthesized copper-tin alloys.

823°C. Above this temperature, as more of α liquefies, there is a remarkable shrinkage, due to the natural collapse of the cylindrical specimen. Besides this, with the formation of a persisting liquid, the specimen is also deformed considerably under the probe-pressure of 28 cN/cm^2 acting on it.

3.3. A2

For 18%Sn alloy, the microstructure, (Fig. 10), shows the presence of massive and slightly rounded dendrites of primary α, on which precipitation of secondary α occurs due to the eutectoid transformation of β to $(\alpha + \gamma)$. This gives rise to a typical kernel-like structure. The surrounding region is occupied by the eutectoid transformation of γ into $(\alpha + \delta)$. This indicates a shift in the composition towards the tin side as the alloy cools, giving rise to the phases in the following order from the core of each dendrite: the primary α, secondary α, eutectoid $(\alpha + \gamma) \rightarrow (\alpha + (\alpha + \delta))$, and eutectoid $(\alpha + \delta)$.

When this alloy is heated again, the DTA plot shows an endothermic reaction at 520°C, with the peak occurring at 527°C. This corresponds to the eutectoid formation (on heating) of $\gamma_{27\%Sn}$ phase from α and δ phases. Between 580°C and 610°C, a very small and gentle hump that is difficult to notice is obtained. This could be due to the formation of β from α and γ. However, this is not certain, as earlier work has established [1] that the heat effect of this eutectoid reaction is possibly extremely small to be detected at this sensitivity. But β does form as can be seen from the microstructures, as well as from the sharp endothermic peak that starts from 790°C, indicating the onset of its liquefaction.

The TMA plot for this alloy, however, shows a small kink—a slight shrinkage—at 520°C corresponding to the formation of a small amount of $\gamma_{27\%Sn}$. This shrinkage is more prominent in the derivative plot (Fig. 7). The formation of β from α & γ, on the other hand does not give any peak. Around 813°C, rapid shrinkage begins, as liquefaction of the alloy begins.

3.4. A3

When the alloy A3 (25.5%Sn), (Fig. 11), is cooled from the molten state, the inevitable super-cooling needed for solidification to begin produces long dendrites of α initially. Some of these dendrites then react with the liquid to form the peritectic β, and later γ. Some of this β further decomposes eutectoidally (on cooling) to give α and γ. The γ (both, the peritectic and the eutectoid γ) then transforms eutectoidally to form α and

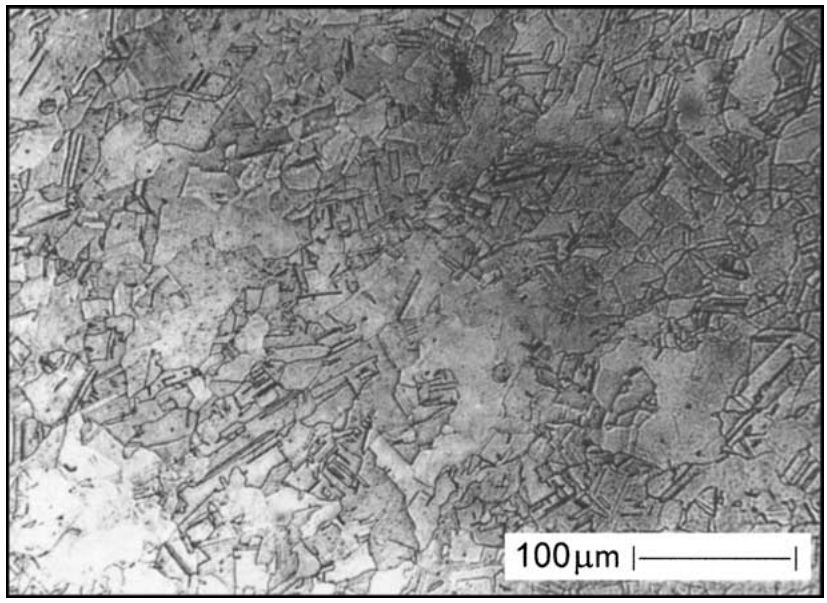

Figure 8 Microstructure of pure electric grade copper (A0) (furnance cooled).

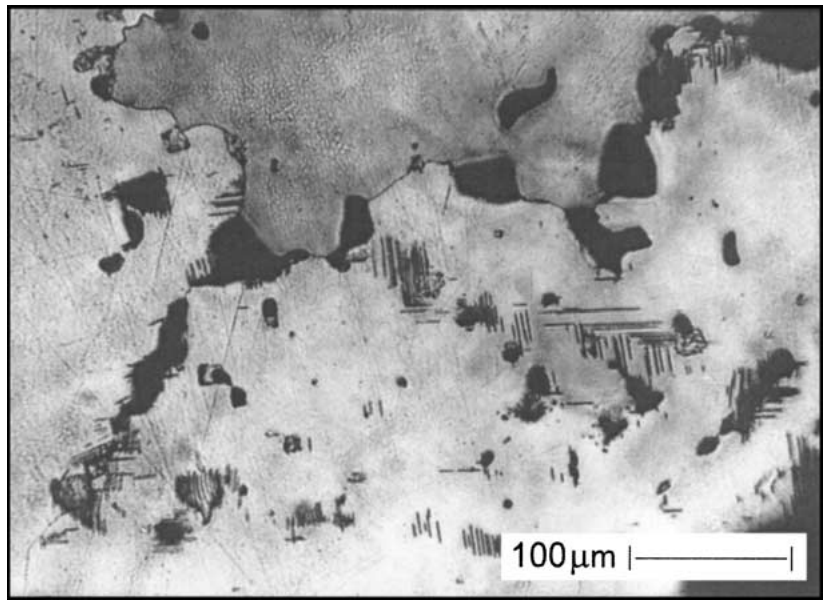

Figure 9 Microstructure of 11 wt%Sn (A1) (furnance cooled).

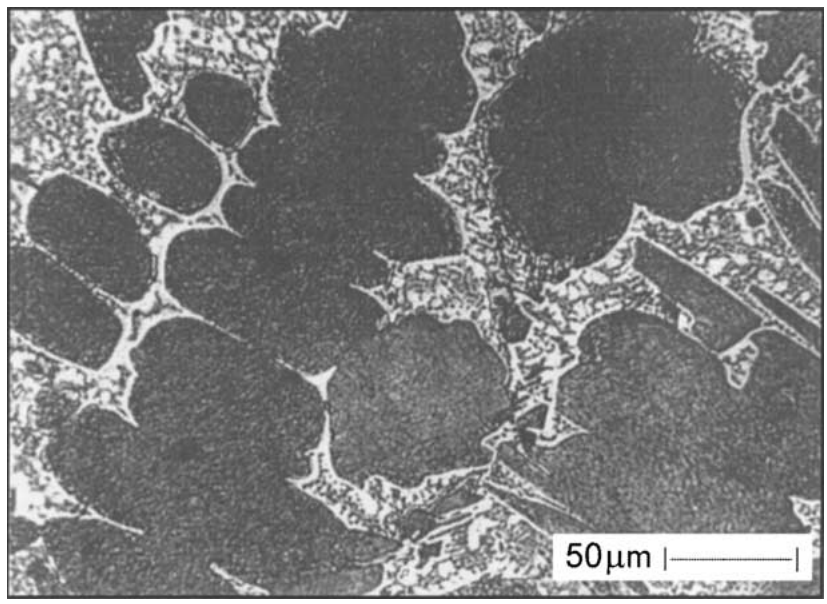

Figure 10 Microstructure of 18 wt%Sn (A2) (furnance cooled).

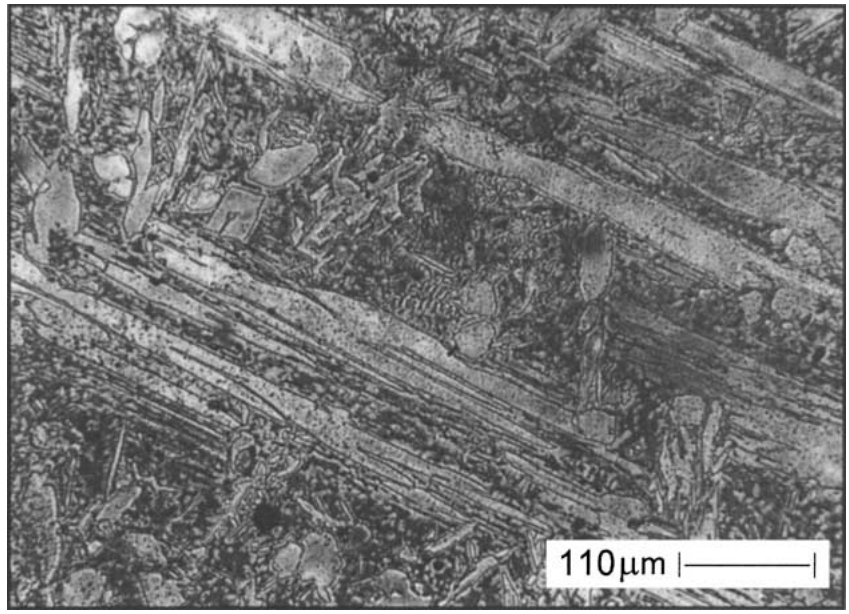

Figure 11 Microstructure of 25.5 wt%Sn (A3) (furnance cooled).

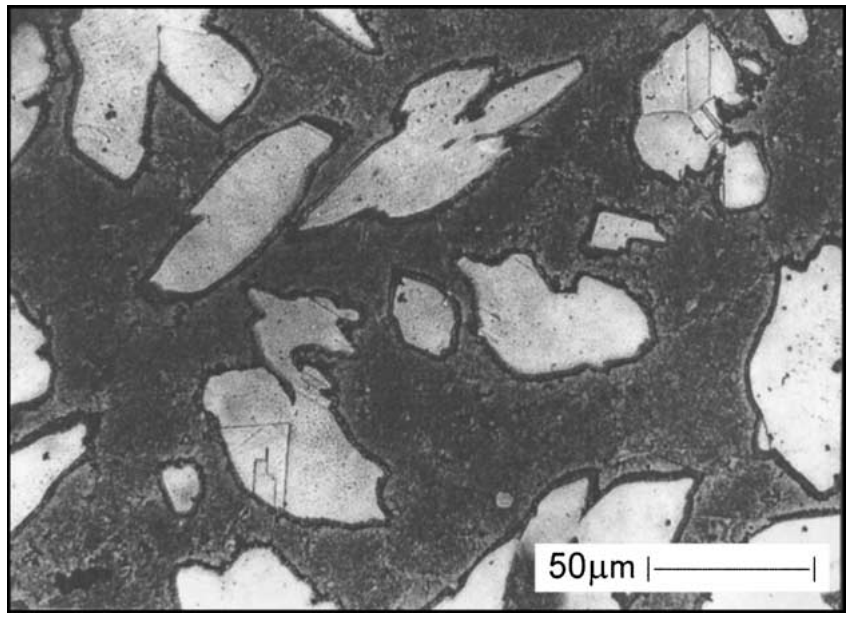

Figure 12 Microstructure of 25.5 wt%Sn (A3) (homogenized).

δ phases, which are seen in the microstructure. There is a slight difference in the morphologies between the $(\alpha + \delta)$ formed from β and that which is formed from γ.

This furnace-cooled microstructure of A3, after being first homogenized at 600°C for 12 hours, and then at 580°C for 8 hours, (Fig. 12), shows the formation of α (lighter phase), around which a dark shell of transformed β (i.e., $\alpha + \gamma$) develops. The remaining region is γ that looks slightly mottled in the microstructure, indicating that some of it has undergone the eutectoid reaction to form $\alpha + \delta$. This is because the quenching, evidently, was not as fast enough as it was intended to be. (Rapidly quenched γ is visually 'plain' [25].)

The DTA plot for the furnace-cooled A3 (plot 4) also shows the reaction $(\alpha + \delta) \rightarrow \gamma_{27\%\mathrm{Sn}}$, giving an endothermic peak at 527°C. Another peak is obtained at 800°C (starting from 790°C) for the liquefaction of β. However, the eutectoid formation of β itself is not seen in the DTA plot.

When this alloy A3 is homogenized at 600°C for 12 hours, followed by another 8 hours at 580°C, DTA (plot 5) detects clearly at 527°C the formation of $\gamma_{27\%\mathrm{Sn}}$ from α and δ. However, the absence of any visible thermal effect of transformation at 586°C again indicates that although the $\alpha + \delta$ were in such a juxtaposition as to form β via the formation of γ, this latter eutectoid reaction could not be detected by DTA. This is in accordance with the observation of earlier workers. Again, on the other hand, the peak that follows indicates that β does form. From the shape of this peak, it is clear that liquefaction of β takes place in two stages: the second close at the heel of the first. Some of this β melts, while the remaining decomposes peritectically.

The TMA plot for furnace-cooled A3 (plot 4) shows shrinkage or an arrest in expansion, at 520°C due to the formation of $\gamma_{27\%\mathrm{Sn}}$. The peak is at 527°C in the derivative plots. There is a slight expansion as the liquefaction of the alloy begins at 800°C, but this is soon followed

by shrinkage as the structure begins to collapse. When this alloy A3 is homogenized at 600°C for 12 hours and then again, at 580°C for 8 hours, the plot shows a remarkable arrest in expansion due to the formation of $\gamma_{27\%Sn}$. The formation of β from α & γ, however, still cannot be seen, though the alloy was heat-treated purposefully to achieve the equilibrium compositions of α and $(\alpha + \delta \rightarrow \gamma_{25\%Sn})$ to react eutectoidally to form β.

3.5. A4

Although the tin in the alloy A4 (28%Sn), (Fig. 13), exceeds the amount that is required for the formation of α on cooling from the liquid state, the microstructure shows the formation of thin α dendrites. This is because of the essential super-cooling before solidification. Meanwhile, the β, which appears on subsequent cooling, first transforms to γ, and finally to $((\alpha + \delta) + \delta)$.

The DTA of this alloy A4 also shows clearly the eutectoid formation of $\gamma_{27\%Sn}$ phase. As there is also γ richer in tin, another peak starts around 750°C, which represents the start of the liquefaction of $\gamma_{28\%Sn}$. By 790°C, the liquefaction is over.

The TMA plot shows the formation of $\gamma_{27\%Sn}$, by its characteristic shrinkage or an arrest in growth, at around 520°C, (indicated by peak at 527°C in the derivative). This is followed by a slight increase in the expansion rate. Liquefaction of the alloy takes place in two stages, as can be seen clearly in the derivative plot. It begins at about 750°C, and then goes through the peritectic reaction at about 765°C, resulting first in a sudden expansion. The liquefaction is very rapid beyond this, as can be seen by the rapid collapse of the specimen.

3.6. A5

For the 32.5%Sn alloy, (Fig. 14), cooling from the liquid state forms dendrites of γ first. This γ then breaks

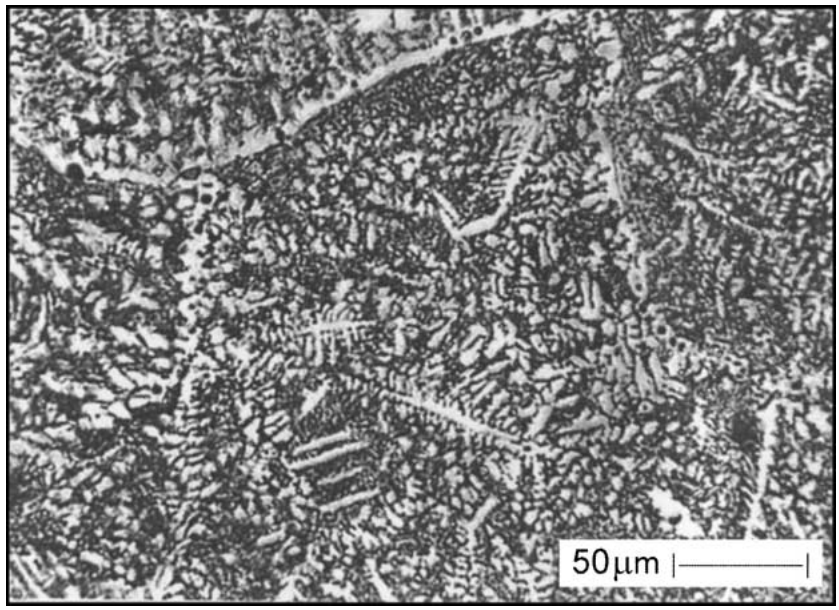

Figure 13 Microstructure of 28 wt%Sn (A4) (furnace cooled).

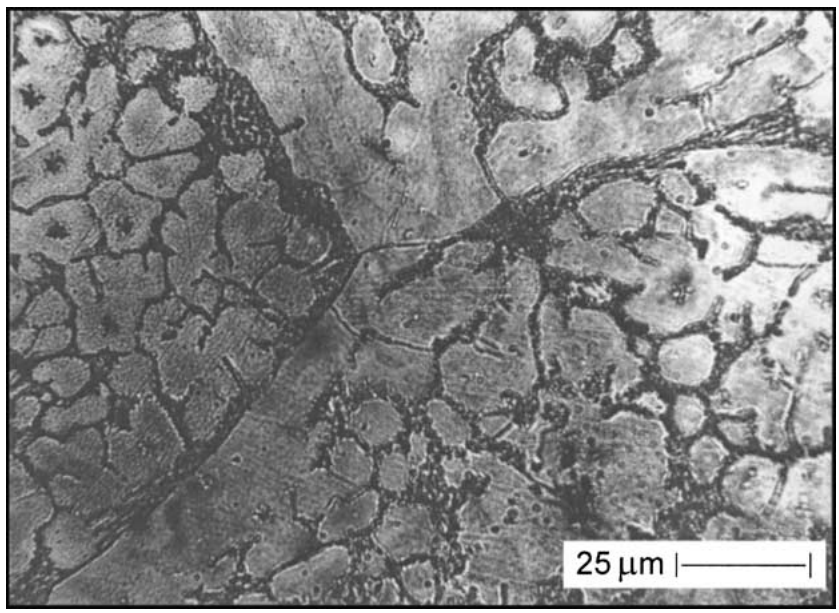

Figure 14 Microstructure of 32.5 wt%Sn (A5) (furnace cooled).

down into α and δ. The primary δ precipitates at the grain boundaries, and the region enclosed in the δ phase network breaks down into $(\alpha + \delta)$ eutectoid, which is very small in amount.

For this alloy, which according to the metallograph is mostly δ with a small amount of $(\alpha + \delta)$ eutectoid, the DTA plot first shows a relatively short peak at about 527°C (starting from 520°C), for the transformation $(\alpha + \delta) \rightarrow \gamma_{27\%\mathrm{Sn}}$. There is absence of any visible thermal effect at 350°C—which is the equilibrium temperature for the formation of eutectoid δ (during heating) from α & ε. This confirms the absence of $(\alpha + \varepsilon)$ which, according to the equilibrium phase diagram, would have formed had δ decomposed eutectoidally during cooling of the alloy from its melt. The kinetics of this decomposition is extremely slow [25]. Thus, for all practical purposes, δ is a 'stable' phase at room temperature. The hump with an apex at 570°C is possibly due to the complete formation of $\gamma_{32.5\%\mathrm{Sn}}$, and the peak at 753°C indicates the liquefaction of this γ.

The TMA of this alloy shows a linear dilation up to 520°C, at which it is arrested owing to the formation of $\gamma_{27\%\mathrm{Sn}}$, which, in accordance with the microstructure, indicates the presence of a small amount of $(\alpha + \delta)$ eutectoid. There is a decrease in the rate of expansion around 595°C, as can be seen clearly in the derivative plot 7 in Fig. 7, indicating the formation of the ζ phase. The expansion rate increases slightly above 710°C, but beyond 750°C, the alloy begins to liquefy rapidly.

3.7. A6

When the tin content is 34%, (Fig. 15), after formation of γ during solidification, the alloy cools through the ζ phase, which gives a lamellar structure of $(\delta + \varepsilon)$ on transforming. A number of cracks are observed as δ as well as ε are hard and brittle intermetallics, and fracture easily during the grinding stage of preparation of the metallographic specimen.

DTA of alloy A6 shows a peak at 585°C due to the eutectoid formation of ζ from $(\delta + \varepsilon)$, large quantities of which were precipitated out during cooling. The small peak around 600°C indicates the peritectoid decomposition of the remaining δ into $(\gamma + \zeta)$. All these processes appear to be endothermic in nature. At 645°C, a peak occurs due to the eutectoid decomposition of ζ into $(\gamma + \varepsilon)$. Liquefaction of $\gamma_{34\%\mathrm{Sn}}$ starts at 720°C giving a peak at 750°C.

The TMA plot for A6 also shows an expansion at 595°C due to the formation of ζ from the $(\delta + \varepsilon)$, though the DTA shows the corresponding reaction temperature of 585°C. At 640°C, there is a remarkable increase in the rate of expansion due to possibly the transformation of $\zeta \rightarrow (\gamma + \varepsilon)$. At 676°C, (derivative plot 8) the rate of expansion decreases probably due to the completion of this peritectoid reaction. At 748°C, there is once again an expansion due to the start of liquefaction of $\gamma_{34\%\mathrm{Sn}}$, and it is followed by shrinkage as the material softens.

3.8. A7

Alloy A7 (38%Sn), (Fig. 16), shows the ε phase that does not undergo any transformation on cooling until room temperature. It is a very brittle inter-metallic, and cracks invariably develop during preparation of the microstructure, as can be seen. The different shades observed are due to the difference in orientation of the grains.

The first peak observed in the DTA plot for this alloy is at 670°C, (starting at 633°C), corresponding to the congruent transformation of ε to γ. This is a structural change. Though the equilibrium temperature for this congruent transformation is reported to be 676°C, it is detected a few degrees early. It is quite likely that the alloy crosses the solvus line to form γ just before the congruent point, as the 38%Sn composition is just outside the ε intermetallic zone at that temperature. Another prominent peak is observed at 743°C (starting at 699°C), corresponding to the liquefaction of $\gamma_{38\%\mathrm{Sn}}$.

In the TMA of this sample A7, there is a massive expansion at around 676°C, due to the congruent transformation of $\varepsilon \rightarrow \gamma_{38\%\mathrm{Sn}}$. This is followed by shrinkage

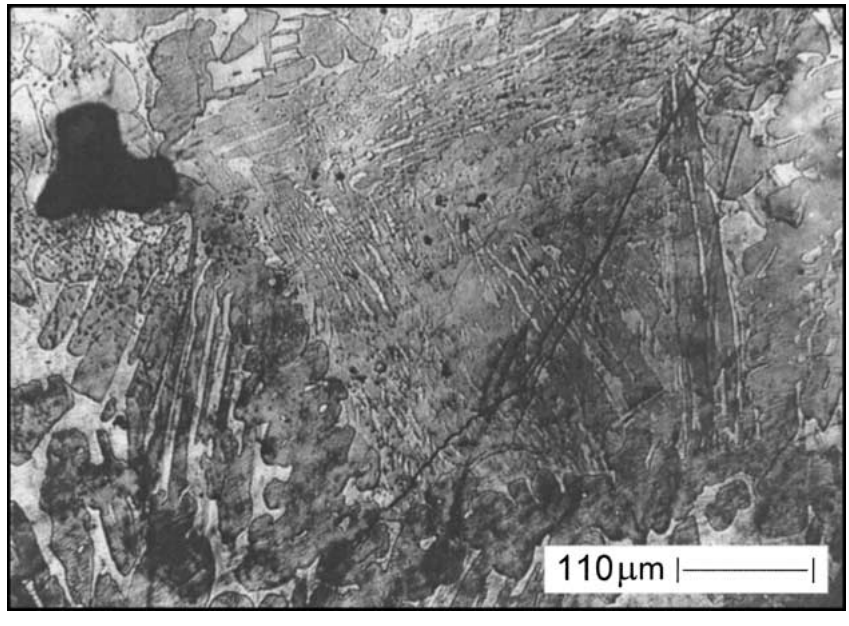

Figure 15 Microstructure of 34 wt%Sn (A6) (furnace cooled).

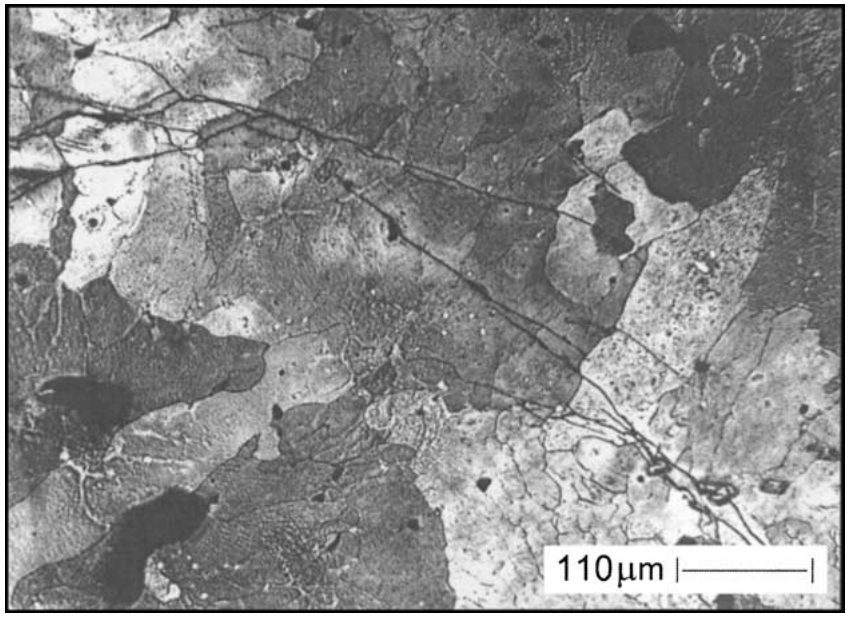

Figure 16 Microstructure of 38 wt%Sn (A7) (furnace cooled).

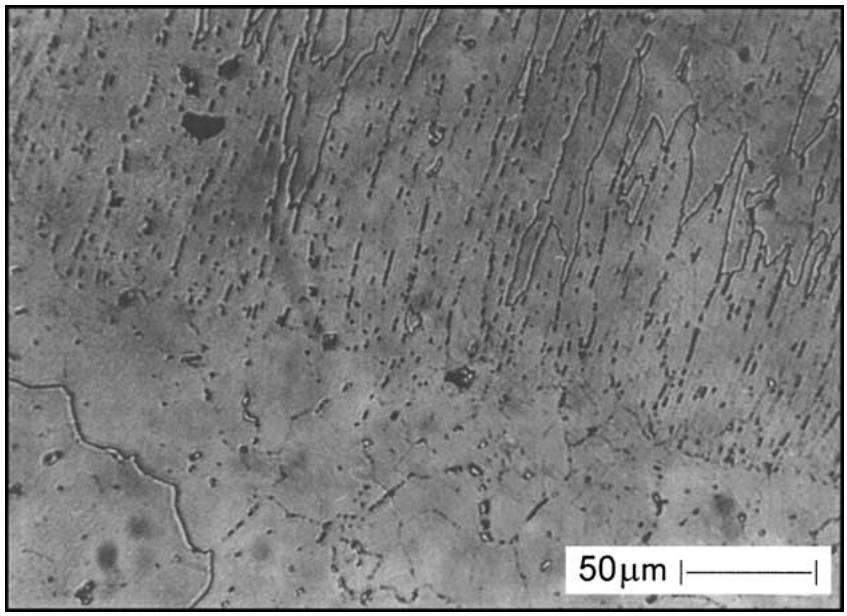

Figure 17 Microstructure of 43 wt%Sn (A8) (furnace cooled).

at 692°C (derivative plot 9), only to be followed by a slight expansion at 735°C as this $\gamma_{38\%Sn}$ begins to liquefy, but soon the specimen begins to collapse rapidly.

3.9. A8

The microstructure of A8 (43%Sn), (Fig. 17), also shows mostly ε, which appears as very fine acicules or dendrites, as the alloy first passes through the precipitation of γ, and then through the metatectic transformation. It is expected that some of this ε reacts with the liquid to form η, but this peritectic is usually slow, and therefore, the alloy solidifies predominantly as ε.

This is confirmed from the DTA of the alloy. No peak is observed for the peritectic decomposition of η to $(\varepsilon + \mathrm{L})$. The peak at 650°C is due to the formation of $\gamma_{42\%Sn}$ by the metatectic reaction. There still remains a good amount of ε that diffuses into liquid and for the γ to shift its composition. The peak at 743°C denotes the liquefaction of this γ whose tin content is probably in the neighbourhood of 40-wt%.

The TMA plot for A8 shows a two-staged expansion starting at 647°C due to the metatectic transformation $\varepsilon + \mathrm{L} \rightarrow \gamma_{42\%Sn}$. The peak for this expansion occurs at 691°C as can be seen from the derivative plot. Soon after 713°C, there is a kink, followed by another expansion due to the start of its liquefaction, $\gamma \rightarrow (\gamma + \mathrm{L})$. This is followed by rapid collapse at 735°C. A point to be noted here is that there is no peak, even in the derivative-curve, for the peritectic decomposition of η to $(\varepsilon + \mathrm{L})$. This confirms that there is no η present in the slow-cooled, or that it is negligibly small to produce any visible effect on thermal analysis.

3.10. A9

When the alloy A9 (50%Sn), (Fig. 18), is furnace-cooled, γ first precipitates out, but a substantial amount of liquid remains before the metatectic transformation

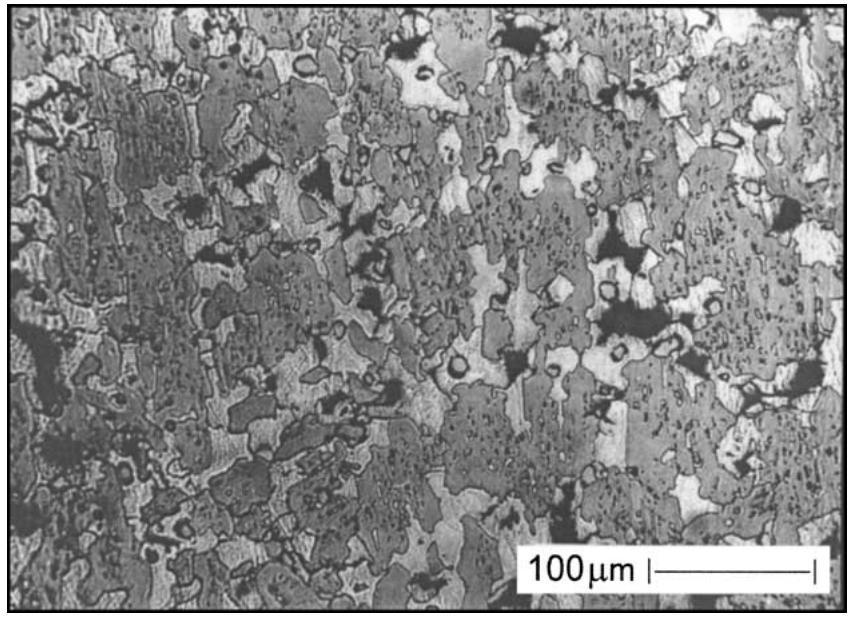

Figure 18 Microstructure of 50 wt%Sn (A9) (furnace cooled).

takes place. This γ in (liquid$_1 + \gamma$) then decomposes metatectically into (liquid$_2 + \varepsilon$), and these two liquids are enriched with tin as the temperature falls. When the peritectic temperature of 415°C is reached, (ignoring the super-cooling that is of course required), the liquid and a part of ε react to form η at the periphery of the ε. Proper etching reveals a lighter phase (η) surrounding a darker phase (ε). Also observed are pores left behind as the 'Cu-enriched' liquid tin solidifies.

The DTA plot for A9 shows a large and broad peak at 420°C denoting, now, the peritectic decomposition of $\eta \rightarrow (\varepsilon + L)$. Around 650°C, (which shows a the peak at the temperature), the formation of $\gamma_{42\%\mathrm{Sn}}$ from ε and liquid by the metatectic reaction takes place. Liquefaction of γ begins at 695°C.

The TMA plot for A9 shows a slightly delayed expansion at 234°C corresponding to the melting of Cu-enriched tin. (This is not detected in the DTA.) An enormous expansion is observed at about 642°C due to the metatectic formation of $\gamma_{42\%\mathrm{Sn}}$ from $\varepsilon + \mathrm{L}$. Subsequently, a rapid shrinkage is observed from 682°C due to liquefaction and consequent collapse of the specimen.

3.11. A10

Alloy A10 (60%Sn), in the furnace-cooled condition, (Fig. 19), shows a similar structure as A9, but with more percentage of η in it. This is because super-cooling brings down the metatectic reaction before the alloy goes through the transformation as described for A9. The microstructure on homogenizing A10 at 390°C for 20 hours shows a large amount of η (lighter phase), and within it islands of ε, (Fig. 20). (The still lighter phase that is observed in small proportion, but uniformly distributed in the matrix, has been found to be a phase with

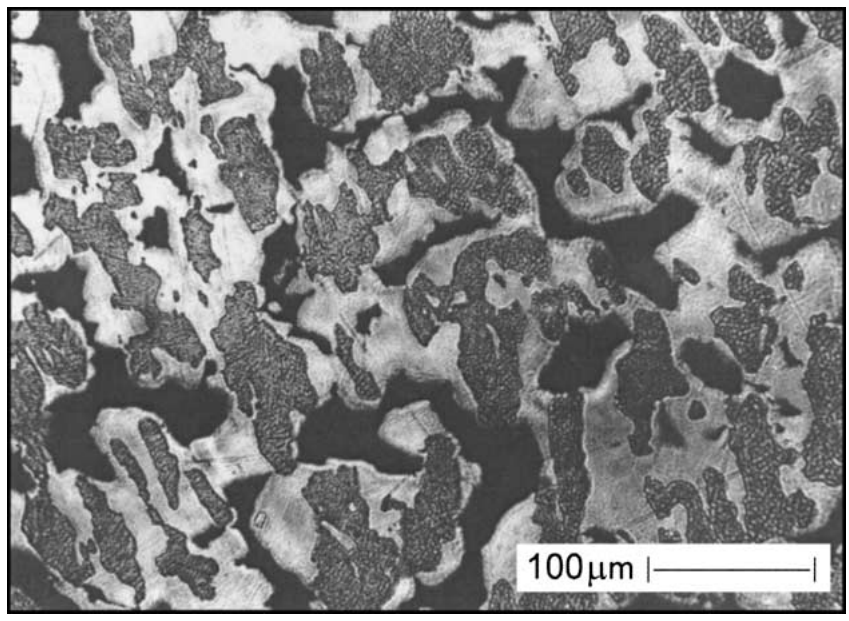

Figure 19 Microstructure of 60 wt%Sn (A10) (furnace cooled).

the impurity lead that is present in the commercial tin used for preparing these alloys.)

DTA of A10 shows a peak at 235°C due to the melting of tin. Between 418°C and 442°C, a very small hump is seen because of the peritectic formation of $(\varepsilon + \mathrm{L})$ from η. This alloy actually has the composition of pure η, and a significant peak is theoretically therefore expected at 415°C due to its transformation peritectically. However, it has been mentioned earlier [25] that pure η is a difficult phase to achieve by casting a melt of that composition, no matter how slowly the cast is cooled. The alloy invariably solidifies as dendrites of ε and tin. A small amount of peritectic η forms at the periphery of these ε dendrites. Very rapid cooling on the other hand only suppresses the formation of η altogether! Thus, as the temperature rises during DTA, this ε goes into liquid, and its complete liquefaction begins a little before 627°C, giving a small hump at that temperature.

However, when this alloy A10 is homogenized at 390°C for 20 hours, the DTA shows first a peak at 235°C corresponding to the melting of tin. (The peak starts a few degrees before 235°C). Unlike the alloy in the furnace-cooled condition, this homogenized sample gives a prominent peak at 446°C (starting from 418°C). This is due to the peritectic decomposition of η to $(\varepsilon + \mathrm{L})$, indicating that substantial amount of η has coagulated during this homogenization, as seen in Fig. 20. Complete liquefaction of the alloy takes place above 650°C.

The TMA plot for A10 in the furnace-cooled condition first shows a prominent flattening at 235°C due to the melting of tin. Secondly, it does not show any dilation due to the reaction $\eta \rightarrow (\varepsilon + \mathrm{L})$, once again confirming that there is very little η in a predominantly ε matrix. The rapid shrinkage from 618°C is due to the liquefaction of the alloy becoming quite significant.

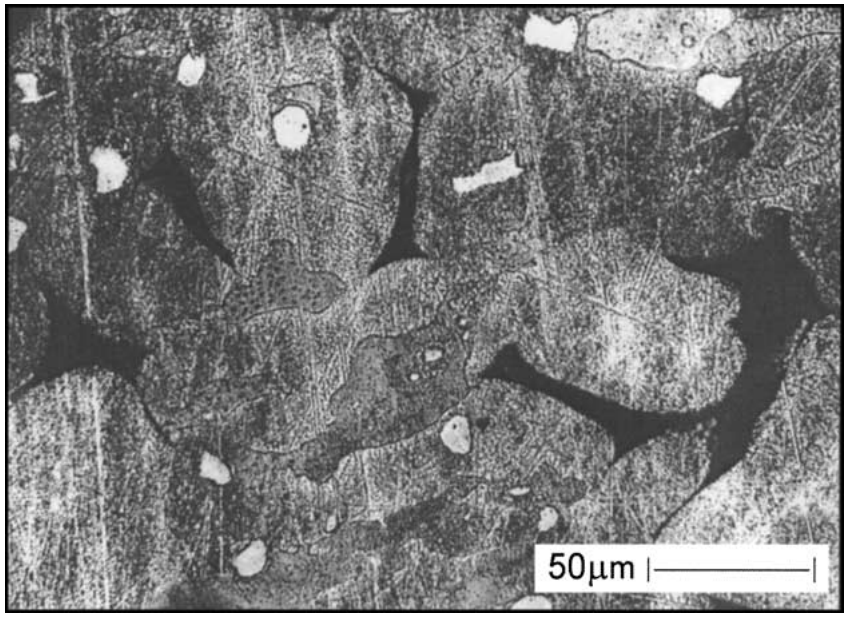

Figure 20 Microstructure of 60 wt%Sn (A10) (homogenized).

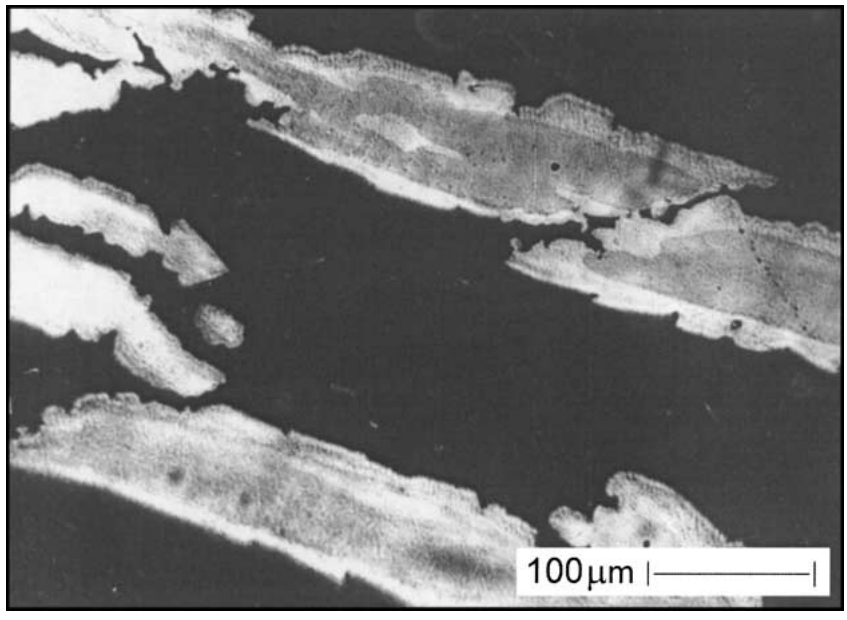

Figure 21 Microstructure of 71, 79, and 90 wt%Sn (A11, A12, A13) (furnace cooled).

Until then, the ε- structure seems to be able to hold the liquid without letting the specimen collapse. It should be noted that complete intrinsic liquefaction takes place at 650°C as shown by DTA.

Even when this alloy is homogenized at 390°C for 20 hours, the derivative shows a very slight softening around 235°C, which indicates a presence of a small amount of Cu-enriched tin that melts. Further, around 420°C the rate of expansion begins to drop, and at about 450°C the expansion is completely arrested. It is quite likely that at this stage, the softening compensates the expansion effect of the peritectic decomposition of η as more liquid is formed. The softening becomes more dominant at 500°C, resulting in rapid shrinkage, and the liquefaction becomes rapid thereafter.

3.12. A11, A12, A13

Alloys A11 (71%Sn), A12 (79%Sn) and A13 (90%Sn), show similar $\eta + \varepsilon$ structures (Fig. 21) as they undergo similar cooling sequence, except that the liquidus is richer in tin respectively. Because of this, dendrites of ε and peripheral η are observed in a tin matrix. The percentage of tin matrix increases from A11 to A13. Sample A13 contains very little ε; it is mostly tin with few dendrites of η.

In the DTA plot for A11, a peak is obtained for the melting of tin. Between 418°C and 440°C, a hump is obtained corresponding to the endothermic reaction $\eta \rightarrow (\varepsilon + \mathrm{L})$. Again, the size of the hump is small, as the alloy is in the furnace-cooled condition. Finally, in the temperature range 495°C to 625°C, a gentle hump is obtained at 598°C, corresponding to the liquefaction of ε. The plot for A12 exhibits a trend similar to that of A11, only the alloy cuts the liquidus much earlier starting at around 520°C.

The DTA of A13 is also similar. This alloy has so little η in it that its effect in DTA is just a small hump in the neighbourhood of 415°C.

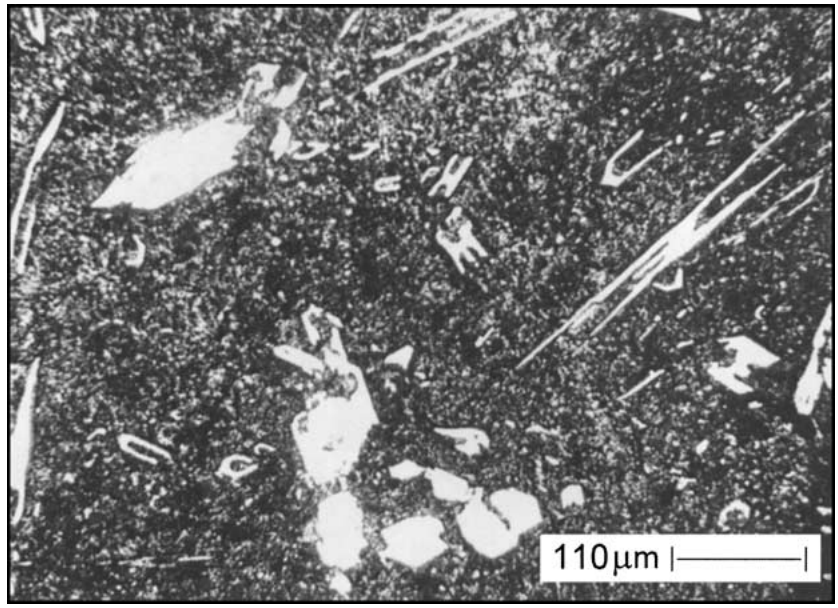

Figure 22 Microstructure of 95 wt%Sn (A 14) (furnace cooled).

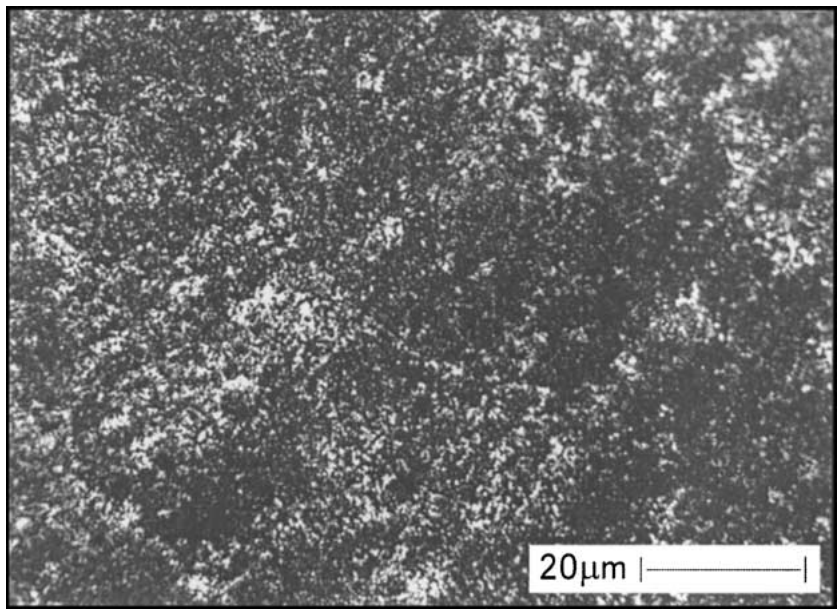

Figure 23 Microstructure of commercially pure tin (A 15) (furnace cooled).

The TMA of alloy A11 shows behaviour similar to that of furnace-cooled A10, except that the peak corresponding to the shrinkage due to melting of tin is visibly more prominent, starting at 230°C. At 430°C, a very small hump is seen in the derivative curve due to the transformation $\eta \rightarrow (\varepsilon + \mathrm{L})$. At around 512°C, rapid shrinkage occurs, due to excessive liquid in the structure.

The alloys A12 and A13 give similar TMA plots. There is a significant shrinkage at about 235°C, due to the melting of tin. The samples thereafter become very soft and collapse under the pressure of the probe on it. The peritectic decomposition of η takes place at 415°C. The final liquefaction takes place around 525°C. The collapse due to excessive liquid in A13 forced an early termination of the TMA run.

3.13. A14

The alloy A14 (95%Sn), (Fig. 22), does not cut the liquidus above the peritectic reaction, and therefore no ε is formed. Only η dendrites are seen in a tin matrix. The DTA plot for A14 shows a similar behaviour, but with no kink for η as the alloy does contain it. The TMA and its derivative show only the melting of the copper-rich tin.

3.14. A15

The microstructure of A15 shows solidified tin (Fig. 23).

The DTA plot for A15 (commercial tin) shows a peak around 235°C corresponding to the melting of tin. There is also a very small peak at 182°C. This temperature coincides with the eutectic temperature of lead-tin alloys that gives further proof that there is trace impurity of lead in the tin that is used for this work.

The TMA plot shows no phase transformation other than tin-liquefaction at about 235°C.

4. Conclusion

1. It is often very difficult to use a multi-property approach on something that can be cooling rate dependent, as it is very difficult to know the real cooling rate the samples experience. It will be different for different apparatus, sample size and geometry. However, in order to study complex system like sintering of a powder metallurgical Cu-Sn powder mix, a multi-property approach has to be adopted, which taking care that all the samples studied in various equipment have been given the same heat-treatment, and have similar thermal geometry. A collective study of metallography, TMA, $\mathrm{d}\Delta L/\mathrm{d}t$ and DTA, therefore, would give advantageous over a study of the alloys carried out separately.

2. From the collective work carried out for this article, the various phase reactions in the Cu-Sn system and their corresponding heat effect and dilation are given in Table I.

3. The formation of β, by the reaction $(\alpha + \gamma) \rightarrow \beta$, does not seem to have any effect on the dilation characteristic of the alloy. It cannot be detected by DTA either.

TABLE I Phase reactions in the Cu-Sn system and their corresponding heat effect and dilation

Temperature range	Reactions during heating	Nature of the DTA peak during heating	Nature of dilation Nature of dilation during heating
232°C	$\mathrm{Sn(S)} \rightarrow \mathrm{Sn(L)}$	endothermic	shrinkage
408–432°C	$\eta \rightarrow (\varepsilon + \mathrm{L})$	endothermic	very small expansion
515°C	$(\alpha + \delta) \rightarrow (\gamma + \delta)$	endothermic	shrinkage
520°C	$\alpha + \delta) \rightarrow \gamma$	endothermic	shrinkage
549°C	$\alpha + \delta) \rightarrow (\alpha + \gamma)$	endothermic	shrinkage
581–618°C	formation of β by $(\alpha + \gamma) \rightarrow \beta$	not detected (probably small)	not detected (probably small)
603°C	$\delta \rightarrow (\gamma + \zeta)$	endothermic	expansion
	$(\gamma + \zeta) \rightarrow \gamma$	endothermic	expansion
638°C	$\zeta \rightarrow (\zeta + \gamma) \rightarrow (\gamma + \varepsilon)$	endothermic	increase in the rate of expansion
642–660°C	$\varepsilon \rightarrow (\varepsilon + \gamma)$	endothermic	expansion
	$(\varepsilon + \gamma) \rightarrow \gamma$	endothermic	expansion
For the formation of any liquid phase a small expansion followed by shrinkage is seen, such as:			
495–598°C	$(\varepsilon + \mathrm{L}) \rightarrow \mathrm{L}$	endothermic	small expansion followed by shrinkage
627°C	$(\varepsilon + \mathrm{L}) \rightarrow \mathrm{L}$	endothermic	small expansion followed by shrinkage
644°C	$\gamma_{50.4\%\mathrm{Sn}} \rightarrow (\gamma + \mathrm{L})$	endothermic	shrinkage
700°C	$\gamma_{43\%\mathrm{Sn}} \rightarrow (\gamma + \mathrm{L})$	endothermic	shrinkage
736°C	$\gamma_{38.5\%\mathrm{Sn}} \rightarrow (\gamma + \mathrm{L})$	endothermic	shrinkage
745°C	$\gamma_{28\%\mathrm{Sn}} \rightarrow (\gamma + \mathrm{L})$	endothermic	small expansion followed by shrinkage
748°C	$\gamma_{34.1\%\mathrm{Sn}} \rightarrow (\gamma + \mathrm{L})$	endothermic	small expansion followed by shrinkage
750–760°C	$\gamma_{32.5\%\mathrm{Sn}} \rightarrow (\gamma + \mathrm{L})$	endothermic	small expansion followed by shrinkage
795°C	$\beta_{25\%\mathrm{Sn}}\} \rightarrow (\beta + \mathrm{L})$	endothermic	small expansion followed by shrinkage
800°C	$\beta \rightarrow \alpha + \mathrm{L}$	endothermic	shrinkage
830–845°C	$\alpha_{17.7\%\mathrm{Sn}} \rightarrow (\alpha + \mathrm{L})$	endothermic	shrinkage
	$\alpha_{11.2\%\mathrm{Sn}} \rightarrow (\alpha + \mathrm{L})$	endothermic	shrinkage
For the peritectic transformation $(\gamma \rightarrow \beta + \mathrm{L})$ and endotherm is seen, accompanied by an expansion or shrinkage depending upon the amount of liquid present. For small amounts: an expansion; and for large amounts; a shrinkage.			

4. The formation of any liquid phase by melting is accompanied by a small expansion followed by shrinkage. Examples of such reactions are:

$$\gamma_{28\%\mathrm{Sn}} \rightarrow (\gamma + \mathrm{L}); \beta \rightarrow (\beta + \mathrm{L}); \quad \text{and} \quad \alpha \rightarrow (\alpha + L).$$

However, if the liquid is forming as the result of a transformation, e.g., $\gamma_{25\%\mathrm{Sn}} \rightarrow (\beta + \mathrm{L})$, the expansion or the shrinkage then depends on the amount of liquid present. If a small amount of liquid is present, there might be an expansion; on the other hand, if the liquid proportion is large, there will be a massive shrinkage due to a collapse of the sample.

For the peritectic transformation $(\gamma \rightarrow \beta + \mathrm{L})$ an endotherm is seen, accompanied by an expansion or shrinkage depending upon the amount of liquid

present. For small amounts: an expansion; and for large amounts: a shrinkage.

References

1. LOEWENDAHL, U. S. Patent 1, 051, 814, (1913). Cited in K. H. Roll, "History of Powder Metallurgy," Metals Handbook, 9th ed. Vol. 7: Powder Metallurgy (American Society for Metals, Metals Park, Ohio, 1984) p. 14.
2. E. G. GILSON, U.S. Patent 1, 179, 407, (1916), Cited in K. H. Roll, "History of Powder Metallurgy," Metals Handbook, 9th ed. Vol. 7: Powder Metallurgy (American Society for Metals, Metals Park, Ohio, 1984) p. 14.
3. E. G. GILSON, *General Electric Review* **24** (1921) 949.
4. R. E. JOHNSON, "Metals Handbook," Vol. 8, 8th ed. (ASM Publishers, Ohio, 1973) p. 299.
5. D. F. BERRY, *Powder Metallurgy* **15** (30) (1972) 247.
6. H. MITANI, *Trans. Japan J. I. M.* **3** (1952) 244.
7. E. PEISSKER, in "Modern Developments in Powder Metallurgy," Vol. 7, edited by H. H. Hausner and W. E. Smith (Princeton, NJ, 1974) p. 597.
8. R. P. KOEHRING, in "Powder Metallurgy," edited by J. Wulff (American Society for Metals, Cleveland, OH, 1942) p. 278.
9. A. BOSE, Ph.D. thesis, Department of Metallurgical Engineering, I. I. T. Kharagpur, India, 1981.
10. N. N. ACHARYA, P. G. MUKUNDA and A. BOSE, *Powder Met. Int.* **16**(5) (1984) 212.
11. N. N. ACHARYA and P. G. MUKUNDA, *Metal Powder Report* **42**(2) (1987) 104.
12. *Idem., The International Journal of Powder Metallurgy* **31**(1) (1995) 63.
13. *Idem., ibid.* **31**(1) (1995) 73.
14. *Idem., ibid.* **31**(1) (1995) 81.
15. N. N. ACHARYA, Ph. D. thesis, Department of Metallurgical Engineering, I. I. T. Kharagpur, India, 1985.
16. N. N. ACHARYA and P. G. MUKUNDA, in Proceedings of the 5th National Symposium on Thermal Analysis, September 1985, p. 3.72.
17. *Idem.,* in Proceedings of the 5th National Symposium on Thermal Analysis, 1985 p. 3.76.
18. K. L. PATEL, *Metal Powder Report* **40**(6) (1985) 358.
19. *Idem., Ibid.* **40**(7/8) (1985) 424.
20. T. KOHNO and M. J. KOCZAK, *Progress in Powder Metallurgy* **38** (1982) 463.
21. P. SAVITISKII, M. A. EMEL'YANOVA and N. N. BURTSEV, *Soviet Powder Metallurgy and Metal Ceramics,* May (1984) 989. [Translated from *Poroshkovaya Metallurgiya* **22**(12(252)) (1983) 30.]
22. N. N. ACHARYA, *J. Mater. Sci. Lett.* **18** (1999) 681.
23. A. HALPERN, "3000 Solved Problem in Physics," Schaum's Solved Problems Series (McGraw-Hill Book Company, 1988) p. 297.
24. N. N. ACHARYA and P. G. MUKUNDA, *Metallography* **21**(2) (1988) 137.
25. E. BERAHA and B. SHPIGLER, "Color Metallography" (ASM, Ohio, 1977).

Received 5 May 2000
and accepted 6 April 2001